NANO LETTERS

pubs.acs.org/NanoLett Letter

Quantum Photonic Circuits Integrated with Color Centers in Designer Nanodiamonds

Kinfung Ngan, Yuan Zhan, Constantin Dory, Jelena Vučković, and Shuo Sun*

Cite This: https://doi.org/10.1021/acs.nanolett.3c02645 Read Online

ACCESS | Metrics & More | Article Recommendations | Supporting Information

ABSTRACT: Diamond has emerged as a leading host material for solid-state quantum emitters, quantum memories, and quantum sensors. However, the challenges in fabricating photonic devices in diamond have limited its potential for use in quantum technologies. While various hybrid integration approaches have been developed for coupling diamond color centers with photonic devices defined in a heterogeneous material, these methods suffer from either large insertion loss at the material interface or evanescent light-matter coupling. Here, we present a new technique that enables the deterministic assembly of diamond color centers in a silicon nitride photonic circuit. Using this technique, we observe Purcell enhancement of silicon vacancy centers coupled to a silicon nitride ring resonator. Our hybrid integration approach has the potential for achieving the maximum possible light-matter interaction strength while maintaining low insertion loss and paves the way toward scalable manufacturing of large-scale quantum photonic circuits integrated with high-quality quantum emitters and spins.

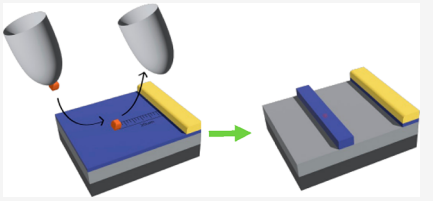

KEYWORDS: *Quantum Optics, Solid-State Quantum Emitters, Integrated Photonics*

Diamond is a unique host material for a diverse range of color centers with remarkable optical and spin coherence.[1,2] This is largely due to its wide bandgap, exceptional chemical stability, and the feasibility of synthesizing single-crystal diamond with extremely low impurities at parts-per-billion level.[3] Groundbreaking proof-of-concept experiments have been reported by employing diamond color centers as single-photon emitters or optically accessible spin qubits, including single-photon generation,[4] entanglement distribution and swapping,[5−7] quantum teleportation,[8] and memory-enhanced quantum communication.[9,10] To improve the performance and scalability of these applications requires the integration of diamond color centers with scalable photonic circuits.[11] However, despite significant advancements in diamond fabrication in the past decade,[12−15] creating large-scale photonic circuits in diamond remains a significant challenge. Additionally, the stochastic nature of color center creation makes it difficult to achieve the scalable and deterministic integration of color centers with photonic circuits.

Hybrid integration, the process of integrating quantum emitters with photonic circuits in a heterogeneous material, provides a viable solution to both aforementioned challenges.[16,17] Hybrid integration allows us to take the best of both worlds: the high-quality quantum emitters and spins based on color centers in diamond, and the wafer-scale integrated photonic circuits in fabrication-friendly materials such as silicon nitride (SiN). In addition, one can use preselected quantum emitters for photonic integration, making hybrid integration a scalable way to assemble complex quantum photonic circuits. Two different approaches have been developed for the hybrid integration of diamond color centers with heterogeneous photonic circuits. The first one relies on the pick-and-place technique,[18,19] where diamond photonic devices containing color centers are picked up from a diamond substrate and placed onto sockets defined on a heterogeneous photonic circuit. This approach allows for the maximum possible coupling between the color center and a diamond photonic device such as a waveguide or a cavity. However, it suffers from a relatively large insertion loss (typically a few dB)[19] at the interface between the diamond waveguide and the photonic circuit, due to a combination of placement errors and photon scattering. The second approach relies on evanescent coupling of diamond color centers with photonic devices defined completely in the heterogeneous material.[20−26] This can be achieved by fabrication of photonic devices in a high-refractive-index material deposited on single-crystal diamond,[20−23] or by placing nanodiamonds on top of a photonic device defined in a heterogeneous material.[23−26] While this approach avoids insertion loss at the material interface, it suffers from weak evanescent coupling between the quantum emitter and the photonic device.

In this article, we report a new hybrid integration approach that has the potential to achieve the maximum possible light-

Received: July 14, 2023
Revised: September 27, 2023

https://doi.org/10.1021/acs.nanolett.3c02645
Nano Lett. XXXX, XXX, XXX−XXX

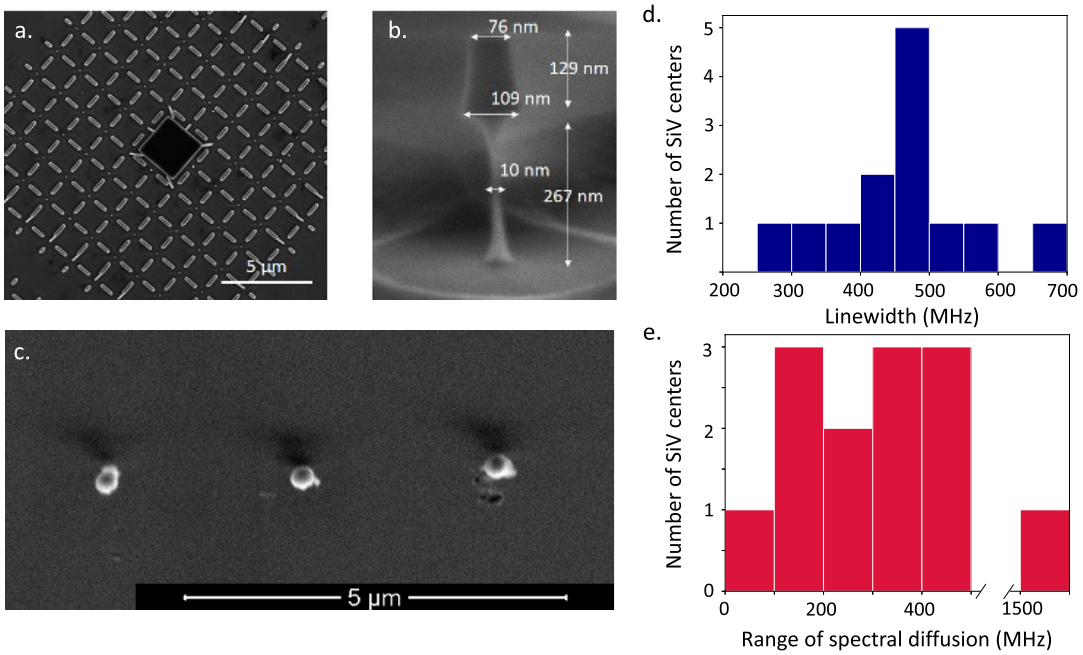

Figure 1. Fabrication, assembly, and characterization of designer nanodiamonds. (a) SEM image of an array of designer nanodiamonds fabricated on a single-crystal diamond substrate. (b) SEM image of the side view of a single designer nanodiamond. (c) SEM image of three designer nanodiamonds deterministically assembled on a thin-film SiN arranged in a line. (d) Histogram of the linewidth of 13 SiV centers in 9 designer nanodiamonds transferred from the diamond substrate to the thin-film SiN. (e) Histogram of the range of spectral diffusion in 10 min of the same 13 SiV centers in 9 transferred designer nanodiamonds.

matter interaction strength while maintaining low insertion loss at the material interface. This approach is achieved by deterministic assembly of nanodiamonds *inside* SiN, followed by fabrication of photonic devices in SiN aligned with the nanodiamonds. Using the new hybrid integration technique, we demonstrate deterministic integration of diamond silicon vacancy (SiV) centers with photonic waveguides and cavities defined in SiN. We also observe Purcell enhancement of SiV centers coupled to a SiN ring resonator. Our hybrid integration technique is not specific to SiV centers or SiN photonics. It is generally applicable to the integration of virtually any solid-state quantum emitter with photonic devices defined in thin-film materials. Our results thus represent an important step toward scalable integration of solid-state quantum emitters with large-scale integrated photonics.

Our hybrid integration approach started with top-down fabrication of nanodiamonds based on electron beam lithography (see Supporting Information Section 1).[27] Compared with other methods such as high-pressure-high-temperature (HPHT) synthesis,[28] top-down fabrication of nanodiamonds enables precise control of the size and shape of each nanodiamond, which is crucial for scalable photonic integration. For this reason, we refer to these nanodiamonds as the designer nanodiamonds. We started with an electronic grade single-crystal diamond from Element Six. Following standard diamond pretreatment based on triacid clean and oxygen plasma etching, the diamond sample was implanted uniformly with $^{28}Si^{+}$ ions at CuttingEdge Ions, and then annealed under vacuum. This process created a uniform distribution of SiV centers inside the diamond with a density that can be controlled by the implantation dose. On this sample, we fabricated an array of nanopillars with a diameter of ∼150 nm and a height of ∼400 nm via electron beam lithography. We then performed partial undercut of the nanopillars by using quasi-isotropic etching of diamond.[13−15] This step created designer nanodiamonds in the shape of a small cylinder (∼130 nm long) sitting on top of a thin neck (∼10 nm thin). Figure 1a and b shows the scanning electron microscopy (SEM) images of the fabricated designer nanodiamonds viewed from the top (Figure 1a) and the side (Figure 1b), respectively.

The partial undercut is essential as it allows us to deterministically break each designer nanodiamond off from the diamond substrate and assemble them one by one on a heterogeneous substrate. In this work, we used a nanoprobe from an SEM integrated Focused Ion Beam (FIB) system for the transfer of designer nanodiamonds, which allowed us to position the designer nanodiamonds while imaging their positions by using the SEM at the same time. As a proof of concept, we were able to assemble three designer nanodiamonds in a line on the thin-film SiN (see Figure 1c for the SEM image).

To examine the properties of the SiV centers inside the designer nanodiamonds, we measured the photoluminescence excitation spectra of 13 SiV centers in 9 designer nanodiamonds transferred on a thin-film SiN. Figure 1d shows the histogram of the measured linewidth of the 13 SiV centers (see Supporting Information Section 2 for the photoluminescence excitation spectrum of each emitter). We measured a linewidth of 290(10) MHz for the narrowest SiV center and a statistical average linewidth of 460(30) MHz for the 13 SiV centers we measured. The average linewidth is 5 times the lifetime-limited value (94 MHz), which could be due to both implantation-induced lattice damage and the proximity to surfaces. This number is comparable to SiV centers monolithically integrated in a diamond photonic crystal, where a statistical average

https://doi.org/10.1021/acs.nanolett.3c02645
Nano Lett. XXXX, XXX, XXX−XXX

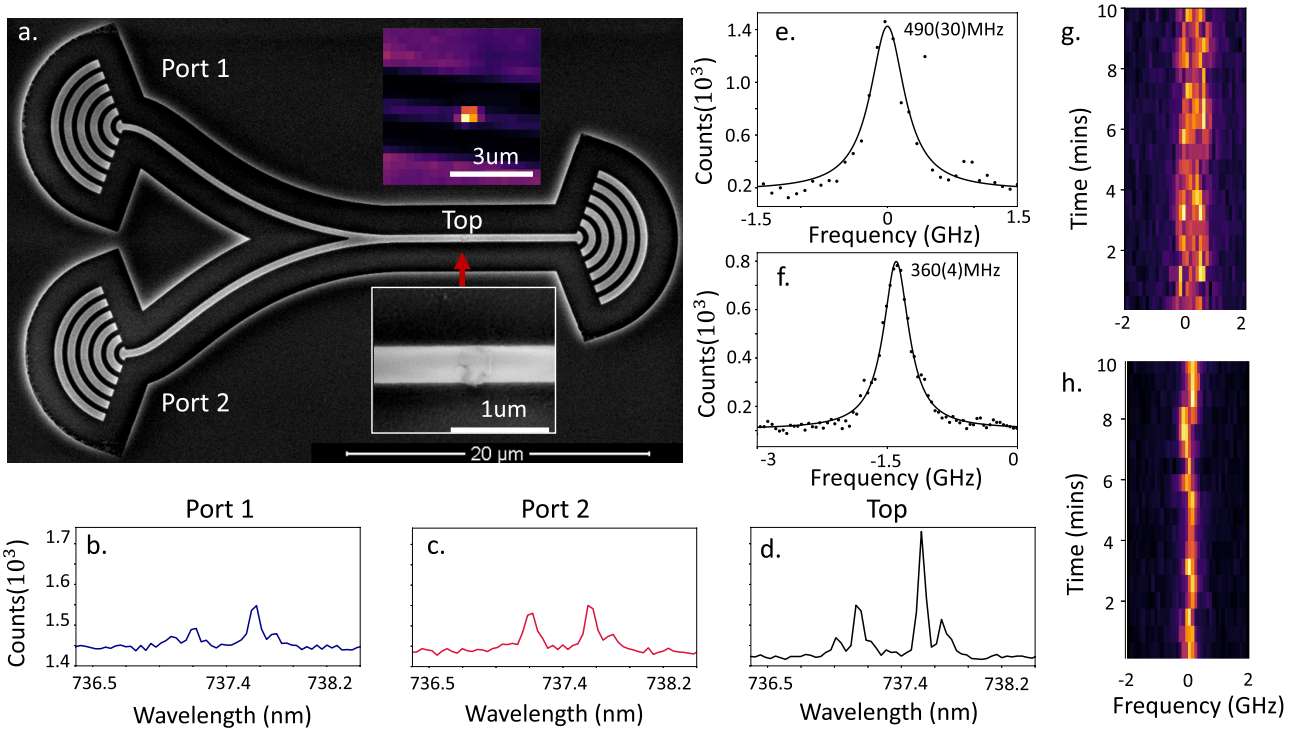

Figure 2. Deterministic photonic coupling between a SiV center in a designer nanodiamond and SiN photonic circuits. (a) SEM image of a SiN photonic circuit integrated with a single designer nanodiamond. The photonic circuit consists of a single nanobeam waveguide coupled to a 50/50 power splitter. The designer nanodiamond is integrated inside the nanobeam waveguide. The bottom inset is an SEM image of a zoomed-in image of the area centered around the designer nanodiamond. The top inset shows the scanning confocal photoluminescence image of the area centered around the designer nanodiamond. (b–d) Photoluminescence spectra of the SiV center collected from output port 1 (b), output port 2 (c), and the top of the integrated designer nanodiamond via free space (d). (e, f) Photoluminescence excitation spectra of the same optical transition from the same SiV center before (e) and after (f) the integration of the designer nanodiamond with the SiN photonics. The black dots show the measured data, and the black solid lines show the Lorentzian fits to the measured data. (g, h) Photoluminescence excitation spectra of the same optical transition shown in (e) and (f) recorded for 10 min before (g) and after (h) the integration of the designer nanodiamond with the SiN photonics. The designer nanodiamond was excited via free space for all spectra.

linewidth of 410(160) MHz was reported.[29] Figure 1e shows the histogram of the range of spectral diffusion in 10 min for the same 13 SiV centers. The majority of the SiV centers had a range of spectral diffusion less than 500 MHz, which is also comparable to SiV centers monolithically integrated in a diamond photonic crystal.[29,30] The similarities of the optical properties between SiV centers in designer nanodiamonds and SiV centers monolithically integrated in diamond nanostructures were expected as the average distance from the SiV center to the surface of the designer nanodiamond is similar to SiV centers in a diamond photonic crystal.[29,30] The spectral stability of the SiV centers could potentially be further improved by Hydrogen plasma treatment of the diamond surface, a technique that was shown effective on SiV centers in HPHT-synthesized nanodiamonds.[31]

The capability of assembling designer nanodiamonds on thin-film SiN enables deterministic hybrid integration of color centers in designer nanodiamonds with SiN nanophotonic devices. We started the hybrid integration by depositing a thin layer of SiN on top of a SiO_2 buffer layer. Following deterministic placement of designer nanodiamonds at the desired locations defined by metal markers patterned on the SiN layer, we deposited a second layer of SiN. This step guarantees that the designer nanodiamonds are buried inside the SiN photonic layer, which enables the maximum possible coupling between the SiV centers and the SiN photonic devices. We then fabricated nanophotonic devices in SiN centered around each designer nanodiamond. We refer the readers to Supporting Information Section 1 for details of the hybrid integration process.

We first demonstrate photonic coupling between a SiV center and a SiN nanobeam waveguide in a photonic circuit. Figure 2a shows the SEM image of a simple SiN photonic circuit integrated with a single designer nanodiamond (as indicated by the small bump in the inset of the SEM image in Figure 2a). The SiN photonic circuit consisted of a nanobeam waveguide connected to a 50/50 power splitter. Each output port of the power splitter was coupled to free space via a grating coupler. It is noteworthy that despite the simplicity of this photonic circuit, fabrication of the same device in diamond for monolithic integration is extremely difficult due to the complex dimensions of the device structure. In contrast, fabrication of this device in SiN is straightforward, and we can follow the hybrid integration process described earlier to incorporate a single designer nanodiamond containing SiV centers into the center of the SiN waveguide, as verified by the scanning photoluminescence microscopy image (top inset of Figure 2a). To confirm waveguide-emitter coupling, we directly excited the designer nanodiamond from the top via free space with a green laser, and collected the photoluminescence of the SiV center from both the top via free space and the two output ports of the 50/50 power splitter.

https://doi.org/10.1021/acs.nanolett.3c02645
Nano Lett. XXXX, XXX, XXX−XXX

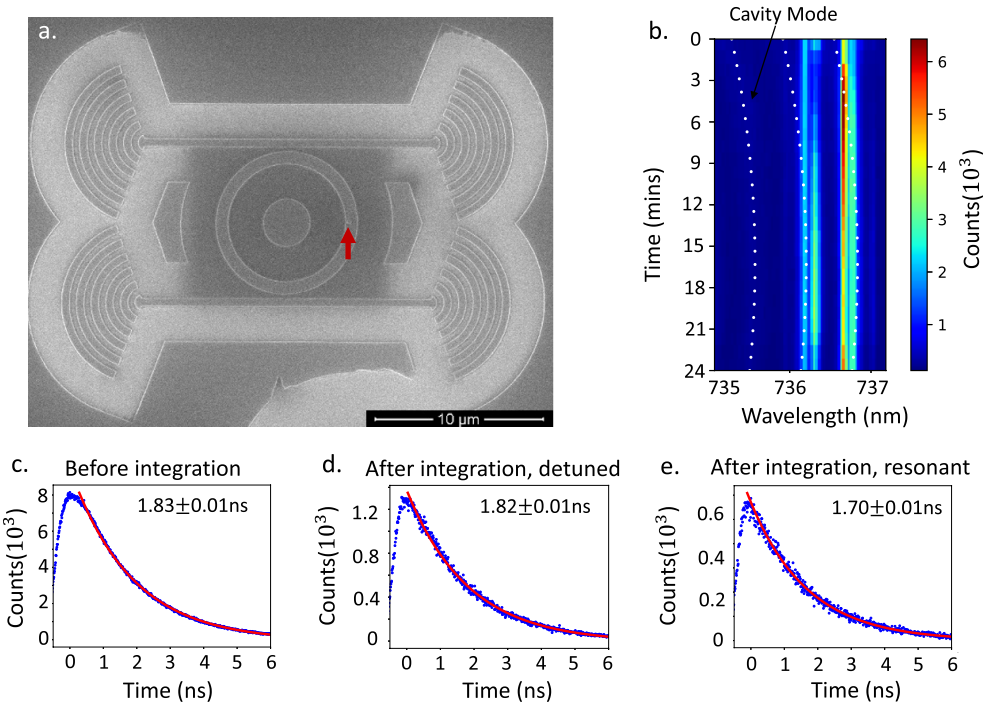

Figure 3. Purcell enhancement of a SiV center induced by a SiN ring resonator. (a) SEM image of the SiN ring resonator integrated with a single designer nanodiamond. The red arrow indicates the position of the integrated designer nanodiamond. (b) Photoluminescence spectra of the SiV center as a function of time. The white dashed lines indicate the resonance of each cavity mode as a function of time (see Supporting Information Section 5 for how we retrieved the cavity resonances). (c–e) Time-resolved photoluminescence of the SiV center before the integration (c), after the integration but with all cavity modes far detuned from any of the four zero-phonon lines (d), and after the integration and with one cavity mode resonant with the transition connecting the lower excited state and the lower ground state (e). The blue dots are the measured data, and the red solid lines are numerical fits to an exponential decay.

The photoluminescence spectra of both output ports (Figure 2b and c) exhibited clear spectral signature of the four zero-phonon lines of the SiV center[32] and were nearly identical with the photoluminescence spectrum observed from the top (Figure 2d), demonstrating photonic coupling between the SiV center and the SiN waveguide.

To examine whether the hybrid integration process degraded the properties of the SiV center, we measured the photoluminescence excitation spectra of a specific optical transition of the SiV center both before (Figure 2e) and after (Figure 2f) hybrid integration. This specific transition connects the lower excited state and the lower ground state of the SiV center, and is conventionally referred to as the C transition. We observed a reduced linewidth from 490(30) MHz to 360(4) MHz. We also measured the range of spectral diffusion by monitoring the photoluminescence excitation spectra of the SiV center over a 10 min interval, both before (Figure 2g) and after (Figure 2h) the hybrid integration process, and observed a qualitatively smaller range of spectral diffusion after the hybrid integration. We attribute the improvement in the optical properties of the SiV center to a more stabilized charge environment at the surface of the designer nanodiamond after the hybrid integration. In particular, we observed significant improvement in the emitter linewidth, emitter blinking, and the range of spectral diffusion for multiple SiV centers after the hybrid integrated sample was at rest for a long time (see Supporting Information Section 3 for details). This observation suggests that the charge environment of the sample near the designer nanodiamond is crucial to maintain the optical coherence of the embedded SiV center.

Building on the capability of deterministic hybrid integration, we now demonstrate Purcell enhancement by the hybrid integration of a SiV center with a SiN ring resonator. Figure 3a shows the SEM image of the SiN ring resonator integrated with a designer nanodiamond. The arrow in Figure 3a indicates the position of the designer nanodiamond. To observe the Purcell effect, we measured the photoluminescence spectra of the SiV center while tuning the cavity resonances via gas condensation (see Supporting Information Section 5 for details of the measurement). Figure 3b shows the measured photoluminescence spectra as a function of time, and the white dashed lines in Figure 3b indicate the resonances of each cavity mode. We observed a 2-time enhancement of emission intensity from the C transition of the SiV center when a cavity mode is resonant with this transition, suggesting cavity induced Purcell enhancement.

To further verify the Purcell effect, we measured the same SiV center before and after its integration with the cavity and compared the measured lifetime directly. Figure 3c–e shows the time-resolved photoluminescence of the SiV center before (Figure 3c) and after (Figure 3d and e) its integration with the SiN ring resonator. In Figure 3d, the cavity modes were off resonant with any of the four zero-phonon lines, and in Figure 3e, one of the cavity modes was resonant with the C transition of the SiV center. The lifetime of the SiV center remained unchanged before and after integration when the cavity modes were off resonant but was reduced by ∼6.5% (5 times of the measurement uncertainty) when a cavity mode was in resonance with the SiV center. We estimated a lower bound of the Purcell factor of 2 by considering a higher bound of the SiV quantum efficiency of 30%, the zero-phonon-line fraction

https://doi.org/10.1021/acs.nanolett.3c02645
Nano Lett. XXXX, XXX, XXX−XXX

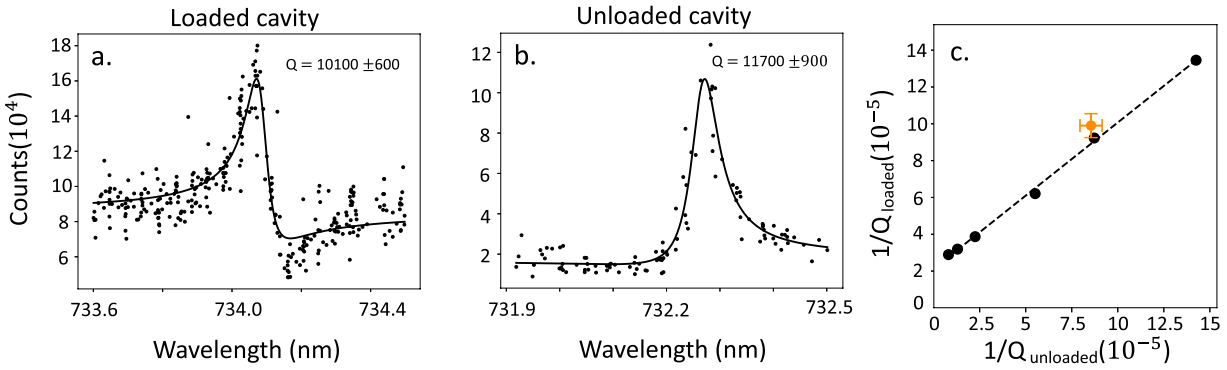

Figure 4. Cavity loss introduced by hybrid integration. (a, b) Transmission spectra of the loaded (a) and unloaded (b) cavity. The black dots are the measured data, and the black solid lines are Lorentzian fits of the measured data from which we derived the Q factor. (c) Calculated values of Q_{loaded} as a function of $Q_{unloaded}$. Here we varied the value of $Q_{unloaded}$ by changing the coupling between the cavity and the bus waveguide. The black dots show the calculated values of Q_{loaded} and $Q_{unloaded}$ for each waveguide-cavity coupling strength, and the black dashed line shows a linear fit. The orange dot indicates the experimentally measured value.

of 80%, and a fraction of 30% of zero-phonon-line emission into the C transition that couples with the cavity (see Supporting Information Section 6 for details of the calculation). The measured Purcell factor is 1/4 of the theoretically attainable value (see Supporting Information Section 7). We attribute the mismatch to the position and polarization misalignment between the emitter and the cavity mode.

A legitimate concern of our hybrid integration approach is that the integration of the designer nanodiamonds may degrade the Q factor of the SiN cavity. The degradation in cavity Q factor can be possibly caused by either the imperfect fabrication in hybrid integration (e.g., the generation of air gaps between the designer nanodiamond and SiN) or the refractive index mismatch between the diamond and the SiN. Here we use Q_{hy} to characterize the Q factor limited by cavity loss induced by the hybrid integration, which satisfies $\frac{1}{Q_{hy}} = \frac{1}{Q_{loaded}} - \frac{1}{Q_{unloaded}}$, where Q_{loaded} and $Q_{unloaded}$ are the Q factors of the cavity with and without the integrated designer nanodiamond, respectively. To experimentally find Q_{hy}, we fabricated two identical cavities on the same wafer by going through the same fabrication run. The only difference between the two cavities was that one cavity was integrated with a designer nanodiamond, whereas the other was not. Figure 4a and b shows the measured transmission spectra of the cavity with (Figure 4a) and without (Figure 4b) the integrated designer nanodiamond. From the cavity transmission spectra, we measured $Q_{loaded} = (1.01 \pm 0.06) \times 10^4$ and $Q_{unloaded} = (1.17 \pm 0.09) \times 10^4$. Based on these measurements, we calculated Q_{hy} to be $Q_{hy} = (7 \pm 5) \times 10^4$.

To further investigate the origin of loss due to hybrid integration, we numerically simulated the Q factor of the loaded cavity (Q_{loaded}) as we varied the Q of the unloaded cavity ($Q_{unloaded}$). Here, we varied $Q_{unloaded}$ by changing the gap distance between the cavity and the bus waveguide. In our simulation, we assumed the designer nanodiamond to be a perfect cylinder, with a diameter of 150 nm and a height of 130 nm, which resembles the shape of the designer nanodiamond used in our experiments. In addition, we assumed no air gaps between the designer nanodiamond and the SiN material. Figure 4c shows the calculated value of Q_{loaded} as a function of the unloaded cavity Q factor $Q_{unloaded}$. By fitting the simulated data to an analytical function of $\frac{1}{Q_{loaded}} = \frac{1}{Q_{hy}} + \frac{1}{Q_{unloaded}}$, we obtained that $Q_{hy} = (4.7 \pm 0.3) \times 10^4$. This value matches our experimentally measured value, suggesting that the main loss induced by hybrid integration is due to the refractive index mismatch between the designer nanodiamond and SiN material. We can potentially reduce the hybrid-integration-induced loss by using smaller designer nanodiamonds or by using a heterogeneous material that has a refractive index closer to diamond (e.g., TiO_2).[33]

In summary, we have reported a new approach for scalable assembly and hybrid integration of diamond color centers with SiN nanophotonic circuits. Our approach has two main potential advantages. First, it is scalable since we can precharacterize each designer nanodiamond and integrate only the desired ones with the photonic device. Second, our approach allows for the maximum possible emitter-light coupling strength and low insertion loss at the material interface. With our current cavity device, when the SiV center is in its excited state, the probability of emitting a photon into a single SiN cavity mode is 6.5%. By employing improved nanofabrication techniques and utilizing smaller designer nanodiamonds, we can improve the photon extraction probability to beyond 97% (see Supporting Information Section 8). It should be noted that nanodiamonds of smaller sizes may adversely affect the coherence properties of the color centers. Therefore, one may need to develop additional surface treatment techniques[31,34] for maintaining the coherence of the color center. The use of cavities with smaller mode volumes may further boost this efficiency if the cavity is designed properly such that the integrated designer nanodiamond does not post a smaller ceiling on the cavity Q factor. In Supporting Information Section 8, we present a specific design of a fishbone photonic crystal cavity that serves for this purpose. The devices reported in this work contain only one designer nanodiamond each. However, the hybrid integration approach that we developed here can be easily extended for the deterministic integration of multiple designer nanodiamonds with the same photonic device. This platform is uniquely suited for studying many-body quantum interactions in an engineerable photonic bath.[35,36] Ultimately, combined with recent progresses in foundry-based large-scale integrated photonics in SiN,[37−39] our hybrid integration approach paves

https://doi.org/10.1021/acs.nanolett.3c02645
Nano Lett. XXXX, XXX, XXX−XXX

the way toward scalable manufacturing of quantum photonic circuits integrated with high-quality quantum emitters and spins.

■ ASSOCIATED CONTENT

Supporting Information

The Supporting Information is available free of charge at https://pubs.acs.org/doi/10.1021/acs.nanolett.3c02645.

Details of nanofabrication, experiments, simulation, and additional supporting data and analysis (PDF)

■ AUTHOR INFORMATION

Corresponding Author

Shuo Sun − *JILA and Department of Physics, University of Colorado, Boulder, Colorado 80309, United States;* orcid.org/0009-0003-9196-8905; Email: shuosun@colorado.edu

Authors

Kinfung Ngan − *JILA and Department of Physics, University of Colorado, Boulder, Colorado 80309, United States*

Yuan Zhan − *JILA and Department of Physics, University of Colorado, Boulder, Colorado 80309, United States;* orcid.org/0000-0001-5450-8879

Constantin Dory − *E. L. Ginzton Laboratory, Stanford University, Stanford, California 94305, United States;* orcid.org/0000-0001-5452-4932

Jelena Vučković − *E. L. Ginzton Laboratory, Stanford University, Stanford, California 94305, United States;* orcid.org/0000-0002-4603-9686

Complete contact information is available at: https://pubs.acs.org/10.1021/acs.nanolett.3c02645

Author Contributions

K.N. and S.S. conceived and designed the experiment. K.N. developed the hybrid integration technique, fabricated the sample, set up and performed the experiments, and analyzed the data. Y.Z. contributed to the setup of the experiment. C.D., under the supervision of J.V., fabricated the designer nanodiamonds sample. S.S. supervised the whole project. All authors participated in the preparation of the manuscript.

Funding

Funding for this work is provided by the National Science Foundation (NSF) (2032567, 2150633, 2317149, and 2326628), the Air Force Office of Scientific Research (AFOSR) (FA2386-21-1-4084), the W. M. Keck Foundation, and the Research & Innovation Office (RIO) Core Facility Assistance Grant Program at the University of Colorado Boulder. Device fabrication was performed, in part, at the Center for Integrated Nanotechnologies, an Office of Science User Facility operated for the U.S. Department of Energy (DOE) Office of Science by Los Alamos National Laboratory (Contract 89233218CNA000001) and Sandia National Laboratories (Contract DE-NA-0003525). The pick-and-place of designer nanodiamonds was performed with the facility at the Colorado Shared Instrumentation in Nanofabrication and Characterization (COSINC): the COSINC−CHR (Characterization) and/or CONSINC-FAB (Fabrication), College of Engineering & Applied Science, the University of Colorado Boulder. The designer nanodiamonds sample was fabricated at the Stanford Nanofabrication Facility (SNF) and the Stanford Nano Shared Facilities (SNSF), supported by the National Science Foundation under award ECCS-1542152. S.S. acknowledges support from the Sloan Research Fellowship.

Notes

The authors declare no competing financial interest.

■ ACKNOWLEDGMENTS

The authors acknowledge Andrew Mounce for fruitful discussions and Yijun Xie and Tomoko Borsa for advice on nanofabrication.

■ REFERENCES

(1) Aharonovich, I.; Greentree, A. D.; Prawer, S. Diamond photonics. *Nat. Photonics* **2011**, *5* (7), 397−405.

(2) Janitz, E.; Bhaskar, M. K.; Childress, L. Cavity quantum electrodynamics with color centers in diamond. *Optica* **2020**, *7* (10), 1232−1252.

(3) Balmer, R.; Brandon, J.; Clewes, S.; Dhillon, H.; Dodson, J.; Friel, I.; Inglis, P.; Madgwick, T.; Markham, M.; Mollart, T.; et al. Chemical vapour deposition synthetic diamond: materials, technology and applications. *J. Phys.: Condens. Matter* **2009**, *21* (36), 364221.

(4) Aharonovich, I.; Castelletto, S.; Simpson, D.; Su, C.-H.; Greentree, A.; Prawer, S. Diamond-based single-photon emitters. *Rep. Prog. Phys.* **2011**, *74* (7), 076501.

(5) Bernien, H.; Hensen, B.; Pfaff, W.; Koolstra, G.; Blok, M. S.; Robledo, L.; Taminiau, T. H.; Markham, M.; Twitchen, D. J.; Childress, L.; Hanson, R. Heralded entanglement between solid-state qubits separated by three metres. *Nature* **2013**, *497* (7447), 86−90.

(6) Hensen, B.; Bernien, H.; Dréau, A. E.; Reiserer, A.; Kalb, N.; Blok, M. S.; Ruitenberg, J.; Vermeulen, R. F.; Schouten, R. N.; Abellán, C.; et al. Loophole-free Bell inequality violation using electron spins separated by 1.3 kilometres. *Nature* **2015**, *526* (7575), 682−686.

(7) Pompili, M.; Hermans, S. L.; Baier, S.; Beukers, H. K.; Humphreys, P. C.; Schouten, R. N.; Vermeulen, R. F.; Tiggelman, M. J.; dos Santos Martins, L.; Dirkse, B.; et al. Realization of a multinode quantum network of remote solid-state qubits. *Science* **2021**, *372* (6539), 259−264.

(8) Pfaff, W.; Hensen, B. J.; Bernien, H.; van Dam, S. B.; Blok, M. S.; Taminiau, T. H.; Tiggelman, M. J.; Schouten, R. N.; Markham, M.; Twitchen, D. J.; Hanson, R. Unconditional quantum teleportation between distant solid-state quantum bits. *Science* **2014**, *345* (6196), 532−535.

(9) Bhaskar, M. K.; Riedinger, R.; Machielse, B.; Levonian, D. S.; Nguyen, C. T.; Knall, E. N.; Park, H.; Englund, D.; Loncar, M.; Sukachev, D. D.; Lukin, M. D. Experimental demonstration of memory-enhanced quantum communication. *Nature* **2020**, *580* (7801), 60−64.

(10) Stas, P.-J.; Huan, Y. Q.; Machielse, B.; Knall, E. N.; Suleymanzade, A.; Pingault, B.; Sutula, M.; Ding, S. W.; Knaut, C. M.; Assumpcao, D. R.; et al. Robust multi-qubit quantum network node with integrated error detection. *Science* **2022**, *378* (6619), 557−560.

(11) O'brien, J. L.; Furusawa, A.; Vučković, J. Photonic quantum technologies. *Nat. Photonics* **2009**, *3* (12), 687−695.

(12) Burek, M. J.; Chu, Y.; Liddy, M. S.; Patel, P.; Rochman, J.; Meesala, S.; Hong, W.; Quan, Q.; Lukin, M. D.; Lončar, M. High quality-factor optical nanocavities in bulk single-crystal diamond. *Nat. Commun.* **2014**, *5* (1), 5718.

(13) Khanaliloo, B.; Mitchell, M.; Hryciw, A. C.; Barclay, P. E. High-Q/V monolithic diamond microdisks fabricated with quasi-isotropic etching. *Nano Lett.* **2015**, *15* (8), 5131−5136.

(14) Mouradian, S.; Wan, N. H.; Schröder, T.; Englund, D. Rectangular photonic crystal nanobeam cavities in bulk diamond. *Appl. Phys. Lett.* **2017**, *111* (2), 021103.

(15) Dory, C.; Vercruysse, D.; Yang, K. Y.; Sapra, N. V.; Rugar, A. E.; Sun, S.; Lukin, D. M.; Piggott, A. Y.; Zhang, J. L.; Radulaski, M.;

et al. Inverse-designed diamond photonics. *Nat. Commun.* **2019**, *10* (1), 3309.
(16) Elshaari, A. W.; Pernice, W.; Srinivasan, K.; Benson, O.; Zwiller, V. Hybrid integrated quantum photonic circuits. *Nat. Photonics* **2020**, *14* (5), 285−298.
(17) Kim, J.-H.; Aghaeimeibodi, S.; Carolan, J.; Englund, D.; Waks, E. Hybrid integration methods for on-chip quantum photonics. *Optica* **2020**, *7* (4), 291−308.
(18) Mouradian, S. L.; Schröder, T.; Poitras, C. B.; Li, L.; Goldstein, J.; Chen, E. H.; Walsh, M.; Cardenas, J.; Markham, M. L.; Twitchen, D. J.; et al. Scalable integration of long-lived quantum memories into a photonic circuit. *Physical Review X* **2015**, *5* (3), 031009.
(19) Wan, N. H.; Lu, T.-J.; Chen, K. C.; Walsh, M. P.; Trusheim, M. E.; De Santis, L.; Bersin, E. A.; Harris, I. B.; Mouradian, S. L.; Christen, I. R.; et al. Large-scale integration of artificial atoms in hybrid photonic circuits. *Nature* **2020**, *583* (7815), 226−231.
(20) Barclay, P. E.; Fu, K.-M.; Santori, C.; Beausoleil, R. G. Hybrid photonic crystal cavity and waveguide for coupling to diamond NV-centers. *Opt. Express* **2009**, *17* (12), 9588−9601.
(21) Gould, M.; Schmidgall, E. R.; Dadgostar, S.; Hatami, F.; Fu, K.-M. C. Efficient extraction of zero-phonon-line photons from single nitrogen-vacancy centers in an integrated gap-on-diamond platform. *Physical Review Applied* **2016**, *6* (1), 011001.
(22) Chakravarthi, S.; Yama, N. S.; Abulnaga, A.; Huang, D.; Pederson, C.; Hestroffer, K.; Hatami, F.; de Leon, N. P.; Fu, K.-M. C. Hybrid Integration of GaP Photonic Crystal Cavities with Silicon-Vacancy Centers in Diamond by Stamp-Transfer. *Nano Lett.* **2023**, *23* (9), 3708−3715.
(23) Radulaski, M.; Zhang, J. L.; Tzeng, Y. K.; Lagoudakis, K. G.; Ishiwata, H.; Dory, C.; Fischer, K. A.; Kelaita, Y. A.; Sun, S.; Maurer, P. C.; et al. Nanodiamond integration with photonic devices. *Laser & Photonics Reviews* **2019**, *13* (8), 1800316.
(24) Fehler, K. G.; Ovvyan, A. P.; Antoniuk, L.; Lettner, N.; Gruhler, N.; Davydov, V. A.; Agafonov, V. N.; Pernice, W. H.; Kubanek, A. Purcell-enhanced emission from individual SiV- center in nanodiamonds coupled to a Si3N4-based, photonic crystal cavity. *Nanophotonics* **2020**, *9* (11), 3655−3662.
(25) Fehler, K. G.; Antoniuk, L.; Lettner, N.; Ovvyan, A. P.; Waltrich, R.; Gruhler, N.; Davydov, V. A.; Agafonov, V. N.; Pernice, W. H.; Kubanek, A. Hybrid quantum photonics based on artificial atoms placed inside one hole of a photonic crystal cavity. *ACS photonics* **2021**, *8* (9), 2635−2641.
(26) Sahoo, S.; Davydov, V. A.; Agafonov, V. N.; Bogdanov, S. I. Hybrid quantum nanophotonic devices with color centers in nanodiamonds. *Optical Materials Express* **2023**, *13* (1), 191−217.
(27) Zheng, J.; Lienhard, B.; Doerk, G.; Cotlet, M.; Bersin, E.; Kim, H. S.; Byun, Y.-C.; Nam, C.-Y.; Kim, J.; Black, C. T.; Englund, D. Top-down fabrication of high-uniformity nanodiamonds by self-assembled block copolymer masks. *Sci. Rep.* **2019**, *9* (1), 6914.
(28) Boudou, J.-P.; Curmi, P. A.; Jelezko, F.; Wrachtrup, J.; Aubert, P.; Sennour, M.; Balasubramanian, G.; Reuter, R.; Thorel, A.; Gaffet, E. High yield fabrication of fluorescent nanodiamonds. *Nanotechnology* **2009**, *20* (23), 235602.
(29) Evans, R. E.; Sipahigil, A.; Sukachev, D. D.; Zibrov, A. S.; Lukin, M. D. Narrow-linewidth homogeneous optical emitters in diamond nanostructures via silicon ion implantation. *Physical Review Applied* **2016**, *5* (4), 044010.
(30) Sipahigil, A.; Evans, R. E.; Sukachev, D. D.; Burek, M. J.; Borregaard, J.; Bhaskar, M. K.; Nguyen, C. T.; Pacheco, J. L.; Atikian, H. A.; Meuwly, C.; et al. An integrated diamond nanophotonics platform for quantum-optical networks. *Science* **2016**, *354* (6314), 847−850.
(31) Rogers, L. J.; Wang, O.; Liu, Y.; Antoniuk, L.; Osterkamp, C.; Davydov, V. A.; Agafonov, V. N.; Filipovski, A. B.; Jelezko, F.; Kubanek, A. Single Si-V- centers in low-strain nanodiamonds with bulklike spectral properties and nanomanipulation capabilities. *Physical Review Applied* **2019**, *11* (2), 024073.
(32) Müller, T.; Hepp, C.; Pingault, B.; Neu, E.; Gsell, S.; Schreck, M.; Sternschulte, H.; Steinmüller-Nethl, D.; Becher, C.; Atatüre, M. Optical signatures of silicon-vacancy spins in diamond. *Nat. Commun.* **2014**, *5* (1), 3328.
(33) Butcher, A.; Guo, X.; Shreiner, R.; Delegan, N.; Hao, K.; Duda III, P. J.; Awschalom, D. D.; Heremans, F. J.; High, A. A. High-Q nanophotonic resonators on diamond membranes using templated atomic layer deposition of TiO2. *Nano Lett.* **2020**, *20* (6), 4603−4609.
(34) Lang, J.; Häußler, S.; Fuhrmann, J.; Waltrich, R.; Laddha, S.; Scharpf, J.; Kubanek, A.; Naydenov, B.; Jelezko, F. *Appl. Phys. Lett.* **2020**, *116* (6), 064001 DOI: 10.1063/1.5143014.
(35) González-Tudela, A.; Hung, C.-L.; Chang, D. E.; Cirac, J. I.; Kimble, H. Subwavelength vacuum lattices and atom-atom interactions in two-dimensional photonic crystals. *Nat. Photonics* **2015**, *9* (5), 320−325.
(36) Douglas, J. S.; Habibian, H.; Hung, C.-L.; Gorshkov, A. V.; Kimble, H. J.; Chang, D. E. Quantum many-body models with cold atoms coupled to photonic crystals. *Nat. Photonics* **2015**, *9* (5), 326−331.
(37) Dong, M.; Clark, G.; Leenheer, A. J.; Zimmermann, M.; Dominguez, D.; Menssen, A. J.; Heim, D.; Gilbert, G.; Englund, D.; Eichenfield, M. High-speed programmable photonic circuits in a cryogenically compatible, visible-near-infrared 200 mm CMOS architecture. *Nat. Photonics* **2022**, *16* (1), 59−65.
(38) Liu, K.; Jin, N.; Cheng, H.; Chauhan, N.; Puckett, M. W.; Nelson, K. D.; Behunin, R. O.; Rakich, P. T.; Blumenthal, D. J. Ultralow 0.034 dB/m loss wafer-scale integrated photonics realizing 720 million Q and 380 μW threshold Brillouin lasing. *Optics letters* **2022**, *47* (7), 1855−1858.
(39) Chanana, A.; Larocque, H.; Moreira, R.; Carolan, J.; Guha, B.; Melo, E. G.; Anant, V.; Song, J.; Englund, D.; Blumenthal, D. J.; et al. Ultra-low loss quantum photonic circuits integrated with single quantum emitters. *Nat. Commun.* **2022**, *13* (1), 7693.

https://doi.org/10.1021/acs.nanolett.3c02645
Nano Lett. XXXX, XXX, XXX−XXX